Postspinning Draw of Polymeric Fibers: Multiscale Micromechanical Model for a Solid Polymer under Finite Deformation and Strain-Induced Crystallization

A. Makradi,[1,2] C. L. Cox,[1,3] S. Ahzi,[1,4] S. Belouettar[5]

[1]*Center for Advanced Engineering Fibers and Films, Clemson University, Clemson, South Carolina 29634*
[2]*Institut Supérieur d'Ingénierie de la Conception, Equipe de Recherche en Mécanique et Plasturgie, 27 Rue d'Hellieule, 88100 Saint-Dié-des-Vosges, France*
[3]*Department of Mathematical Sciences, Clemson University, Clemson, South Carolina 29634*
[4]*University Louis Pasteur, Institut de Mécanique des Fluides et des Solides-Unité Mixte de Recherche 7507, Strasbourg, France*
[5]*Laboratoire de Technologie Industriel, Centre Henri Tudor, 70 Rue de Luxembourg, L-4221 Esch-sur-Alzette, Luxembourg*

Received 11 January 2005; accepted 25 April 2005
DOI 10.1002/app.22766
Published online in Wiley InterScience (www.interscience.wiley.com).

ABSTRACT: A polymeric fiber postspinning draw model is developed. The fiber is stretched between the take-up roll and the draw roll and then relaxed between the draw roll and the relax roll. The behavior of the polymeric material is described by a cooperative elastic–viscoplastic model for a wide range of temperatures and strain rates. The profiles of the fiber velocity, stress, strain rate, and temperature between the different rolls are simulated via the coupling of the cooperative model with the mass, momentum, and energy equations and the boundary conditions. Simulations are conducted with the finite-element method. The computed results show an increase in the fiber stress between the take-up roll and the draw roll due to the molecular orientation and the increase in the crystallization percentage. The sliding distance of the fiber on the draw roll is related to the draw ratio and fiber stiffness. A dramatic drop in the fiber strain rate on the draw roll leads to relaxation of the intermolecular resistance followed by a freeze of the fiber structure when the strain rate vanishes to zero on the draw roll and between the draw roll and the relax roll. © 2006 Wiley Periodicals, Inc. J Appl Polym Sci 100: 2259–2266, 2006

Key words: crystallization; fibers; isotactic; processing; poly(propylene) (PP); strain

INTRODUCTION

For many industrial applications, the utilization of polymers is generally determined by the mechanical response of these materials within a large domain of temperatures and strain rates. The final mechanical and optical properties of a polymeric fiber or film are strongly influenced by the postspinning draw. In fiber and film manufacturing processes, polymeric fibers and films are drawn through a series of rollers to improve their mechanical and optical properties. The behavior of polymeric materials in this process is strongly affected by the stress level, rate of loading, and temperature. The rate and temperature effects are closely related to thermally activated micromechanical processes.[1] A temperature- and strain-rate-dependent cooperative model developed by Richeton et al.[2,3] is used in this work to relate the macroscopic elastic–viscoplastic finite deformation of polymeric materials during the postprocessing to the micromechanical behavior of these materials under large deformation.

This article focuses on the modeling of the postspinning draw of fibers during the fiber-spinning process. Work on the fiber-drawing process under isothermal conditions was reported by Bechtel et al.[4,5] In their modeling, the elastic–plastic constitutive equation is assumed to be independent of the temperature and strain rate. Figure 1 presents a schematic of the fiber-spinning process. In the postdrawing stage of this process, the fibers are stretched between the take-up roll and the draw roll at a temperature above the glass temperature and then relaxed between the draw roll and the relax roll. To model this process, mass, momentum, and energy equations are coupled with a polymeric constitutive equation and boundary conditions (see the Governing Equations section). The numerical simulation is made possible by means of the finite-element method.

GOVERNING EQUATIONS

In the postspinning draw stage of the fiber-spinning process, the polymeric fiber is fully solid, and the

Correspondence to: A. Makradi (Makradi@imfs.u-strasbg.fr).

Contract grant sponsor: National Science Foundation (through the Engineering Research Center program with Clemson University); contract grant number: EEC-9731680.

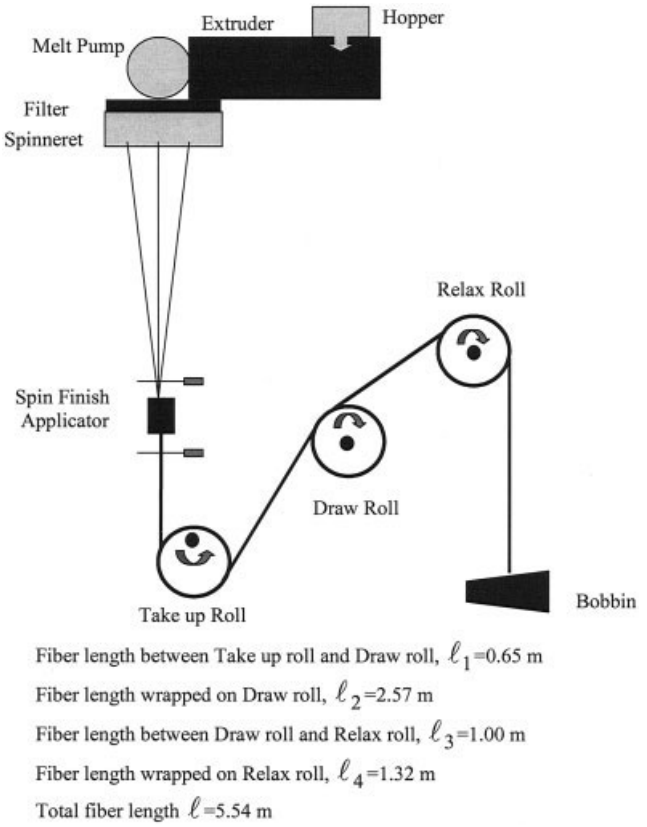

Figure 1 Schematic of the fiber-spinning process.

variation of the radial temperature can be assumed to be constant. The fiber conduction heat transfer is neglected. Therefore, the fiber axial velocity and temperature are assumed to be uniform over the fiber cross section. The fundamental steady-state one-dimensional equations governing the fiber's postspinning draw can be obtained by the radial averaging of the continuity, momentum, and energy balances in a cylindrical coordinate system.[6] The fiber is assumed to be axisymmetric on the rolls.

Mass balance

In a one-dimensional model, the mass balance equation can be written as follows:

$$W = \rho A v_z \tag{1}$$

where W is the mass flow rate, $A = (\pi D^2)/4$ is the fiber cross section, D is the fiber diameter, ρ is the polymer density (assumed to be constant in this study), and v_z is the fiber axial velocity.

Momentum balance

Neglecting the aerodynamic drag and gravity on the filament, we can write the force balance in the following form:

$$W\frac{dv_z}{dz} = \frac{d}{dz}[A(T_{zz} - T_{rr})] + \frac{1}{2}\pi s\frac{dD}{dz} + f\frac{T_{\text{init}}}{(T_{zz} - T_{rr})} \times \left(\frac{Wv_R - Wv_z}{r_0}\right) \tag{2}$$

where the term on the left-hand side is the inertia. On the right-hand side, the first term is the axial variation of the average tensile force, $F = A(T_{zz} - T_{rr})$, where T_{zz} and T_{rr} are the axial and radial components of the Cauchy stress tensor (see the Finite Deformation section) and $T_{zz} - T_{rr}$ is the fiber equivalent stress. The second term is the force related to the action of the surface tension, s. The third term represents the friction between the fiber and the rolls. The parameter T_{init} is the fiber equivalent stress at the take-up roll (i.e., the initial stress corresponding to the stress developed in the spin line between the spinneret and take-up roll). As for the other parameters, v_R is the roll velocity, r_0 is the roll radius, and f is the friction coefficient. This term represents the projection of the resultant force between the fiber centrifugal force and the reaction force of the roll on the fiber. This term is divided by the equivalent stress $(T_{zz} - T_{rr})$ to take account of the stiffness of the fiber; the stiffer the fiber is, the weaker its adhesion becomes to the roll.

Energy equation

The conservation of energy can be written as follows:

$$\rho C_p v_z\frac{d\theta}{dz} = -\frac{4}{D}h(\theta - \theta_a) + (T_{zz} - T_{rr})\frac{dv_z}{dz} + \rho\Delta H_f\frac{d\phi}{dz} \tag{3}$$

where θ_a is room temperature. In the left-hand-side term, the heat capacity, C_p, is a function of the absolute degree of crystallinity, ϕ, and the temperature: $C_p = C_s\phi + C_\ell(1 - \phi)$, where C_s and C_ℓ are the heat capacities of the crystalline phase and the amorphous phase, respectively. These parameters are represented as quadratic functions of temperature θ (°C) as follows:[7]

$$C_s(\theta) = C_{s1} + C_{s2}\theta + C_{s3}\theta^2; \qquad C_\ell(\theta) = C_{\ell 1} + C_{\ell 2}\theta + C_{\ell 3}\theta^2 \tag{4}$$

The first term on the right-hand side is the convective-heat-transfer term between the fiber and the quench air, with h being the convective-heat-transfer coefficient. h is controlled by the fiber diameter, fiber velocity, and temperature-dependent physical properties of the cooling medium:[8]

$$h = 0.42\lambda_s\nu_s^{-0.334}D^{-0.666}v_z^{0.334}[1 + (8v_y/v_z)^2]^{0.167} \tag{5}$$

where v_y is the transverse velocity of the cooling medium, λ_s is the local heat conductivity, and v_s is the local kinematic viscosity. In the dry air, at atmospheric pressure, as a cooling medium, λ_s and v_s are expressed as follows:[8]

$$\lambda_s = 4.49 \times 10^{-5}\theta_f^{0.866} \quad (\text{cal m}^{-1}\,\text{s}^{-1}\,^{\circ}\text{C}^{-1})$$

$$\nu_s = 1.446 \times 10^{-9}\frac{\theta_f^{1.5}}{\theta_f + 113.9} \quad (\text{m}^2\,\text{s})$$

where θ_f is defined as the arithmetic mean of the fiber temperature and quench air temperature.

The second term on the right-hand side of eq. (3) is the viscous dissipation, and the last term is related to the release of latent heat, where ϕ is the average absolute degree of crystallinity. The heat of crystallization per unit of mass, ΔH_f, is expressed as function of temperature θ (°C) as follows:[7]

$$\Delta H_f(\theta) = \Delta H_f(0) + (C_{\ell 1} - C_{s1})\theta + (C_{\ell 2} - C_{s2})\frac{\theta^2}{2} + (C_{\ell 3} - C_{s3})\frac{\theta^3}{3} \quad (6)$$

In eq. (3), the friction heat on the roller is neglected.

Constitutive equation

The temperature- and strain-rate-dependent cooperative model for the determination of the yield stress is used to describe the finite-deformation behavior of polymeric materials.[3] In this work, we briefly address the cooperative model; for more detail, we refer the reader to ref. 3. The cooperative model is based on the idea that the yielding is triggered when an ensemble of polymer chain segments move cooperatively at the same time. To take into account the significance of the activation volume during the yield process, Fotheringham and Cherry[9] introduced the concept that yielding involves a cooperative motion of polymer chain segments. According to the strain-rate/temperature superposition principle,[10] a recent development of the cooperative model[3] has shown that this type of model predicts the yield stress for a wide range of strain rates (low to high) and for a wide range of temperatures (below and above the glass-transition temperature). The resulting model is an Eyring-like equation in which the hyperbolic sine function is raised to the nth power.[11] When the internal stress is neglected, the plastic shear flow increment $\dot{\gamma}^p$ is expressed as follows:

$$\dot{\gamma}^p = \dot{\gamma}^*(\theta)\sin\text{h}^n\left(\frac{V}{2k\theta}(\sqrt{3}\tau)\right) \quad (7)$$

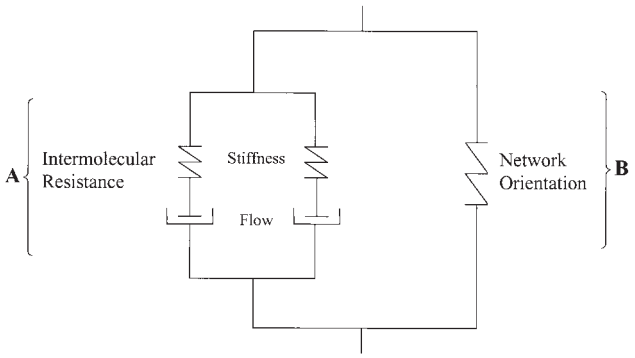

Figure 2 Schematic representation of the breakdown of the total resistance into intermolecular resistance **A** acting in parallel with network resistance **B**.

where k is the Boltzmann's constant, V is the activation volume, n is an activation parameter, and τ is the effective shear stress. The characteristic shear strain rate, $\dot{\gamma}^*(\theta)$, is thermally activated and is given by

$$\dot{\gamma}^*(\theta) = \dot{\gamma}_0\exp\left(-\frac{\Delta H_\beta}{k\theta}\right) \quad (8)$$

where $\dot{\gamma}_0$ is a constant pre-exponential shear strain rate and ΔH_β is the β-activation energy.

Finite deformation

The three-dimensional constitutive model for large deformation behavior is based on the work of Boyce et al.[12] and Ahzi et al.[13] The analog representation considers intermolecular resistance (resistance **A**) acting in parallel with network resistance (resistance **B**; see Fig. 2). The total imposed deformation gradient, **F**, is identical to both the intermolecular deformation gradient, $\mathbf{F}_A$, and the network deformation gradient, $\mathbf{F}_B$ ($\mathbf{F} = \mathbf{F}_A = \mathbf{F}_B$), and the total Cauchy stress tensor, **T**, is the sum of the intermolecular Cauchy stress, $\mathbf{T}_A$, and the network Cauchy stress, $\mathbf{T}_B$ ($\mathbf{T} = \mathbf{T}_A + \mathbf{T}_B$). The velocity gradient is $\mathbf{L} = \dot{\mathbf{F}}\mathbf{F}^{-1} = \mathbf{D} + \mathbf{W}$, where **D** is the rate of deformation and **W** is the spin. The velocity gradient tensor of uniaxial extension is given by

$$\mathbf{L} = \begin{bmatrix} -\nu\dot{\varepsilon}_{\text{eq}} & & \\ & -\nu\dot{\varepsilon}_{\text{eq}} & \\ & & \varepsilon_{\text{eq}} \end{bmatrix} \quad (9)$$

where ν is the Poisson ratio and $\dot{\varepsilon}_{\text{eq}} = dv_z/dz$ is the equivalent strain rate. In this work, we briefly address the contributions of the network resistance [see the Network Resistance (Resistance **B**) section] and the intermolecular resistance [see the Micromechanics of the Two Phases and Averaging Schemes (Resistance **A**) section] because the details can be found in the

literature (Ahzi et al.,[13] Boyce et al.,[12] and Arruda and Boyce[14,15]).

Micromechanics of the two phases and averaging schemes (resistance A)

The intermolecular resistance analog representation (see Fig. 2) is composed of amorphous-phase resistance acting in parallel with crystalline-phase resistance (Ahzi et al.[13] This assumption is equivalent to $\mathbf{F}_A = \mathbf{F}_A^c = \mathbf{F}_A^a$, where $\mathbf{F}_A$, $\mathbf{F}_A^c$, and $\mathbf{F}_A^a$ are the intermolecular, crystalline-phase, and amorphous-phase deformation gradients, respectively.

The crystalline and amorphous deformations can be decomposed into elastic and plastic components via the multiplicative decomposition of the deformation gradient: $\mathbf{F}_A^c = (\mathbf{F}_A^c)^e(\mathbf{F}_A^c)^p$ and $\mathbf{F}_A^a = (\mathbf{F}_A^a)^e(\mathbf{F}_A^a)^p$. The elastic and plastic deformation gradients of both the crystalline and amorphous phases can be further decomposed into a stretch ($\mathbf{V}$) and rotation ($\mathbf{R}$). For instance, $(\mathbf{F}_A^i)^e = (\mathbf{V}_A^i)^e(\mathbf{R}_A^i)^e$, where superscript i represents the phases ($i = a$ or c).

The intermolecular Cauchy stress tensors for the crystalline and amorphous phases are constitutively related to their corresponding elastic stretch tensors, $\mathbf{V}_A^{a,c}$: $\mathbf{T}_A^{a,c} = 1/J\mathbf{C}^{a,c}[\ln((\mathbf{V}_A^{a,c})^e)]$, where $\mathbf{C}^{a,c}$ represents the amorphous and crystalline fourth-order elastic stiffness tensors. Finally, the total intermolecular Cauchy stress tensor, $\mathbf{T}_A$, is given by the rule of mixture:

$$\mathrm{T}_A = \phi\mathbf{T}_A^c + (1-\phi)\mathrm{T}_A^a \tag{10}$$

where ϕ is the volume fraction of the crystalline phase.

The explicit method for the calculation of the amorphous-phase and crystalline-phase Cauchy stresses at each element can be summarized as follows:

Do Loop $\mathbf{F}_t$ and $\mathbf{F}_{t+\Delta t}^p$ are known.

$$\mathbf{F}_{t+\Delta t} = \mathbf{F}_t + \mathbf{L}\mathbf{F}_t \times \Delta t$$

$$\mathbf{F}_{t+\Delta t}^e = \mathbf{F}_{t+\Delta t}\mathbf{F}_{t+\Delta t}^{p-1}$$

$$\mathbf{T}_A = \frac{1}{J}C\{\ln[(\mathbf{V}_A)^e]\}$$

(the calculated stresses)

$$(\mathbf{V}_A)^e = [\mathbf{F}_{t+\Delta t}^e(\mathbf{F}_{t+\Delta t}^e)^T]^{1/2}$$

$$\mathbf{F}_{t+\Delta t}^p = \mathbf{F}_t^p + \mathbf{D}^p\Delta t$$

(update the plastic gradient of the deformation for the next time step)

$$\mathbf{D}^p = \frac{\dot\gamma}{\tau\sqrt{2}}\mathbf{T}_A'$$

where

$$\tau = \sqrt{\frac{1}{2}\mathbf{T}_A'\mathbf{T}_A'}$$

End Loop $\mathbf{T}_A'$ is the deviatoric Cauchy stress.

Network resistance (resistance B)

The Cauchy stress representing the network resistance can be determined by statistical rubber–elastic theory based on the eight-chain model of Arruda and Boyce.[14,15] This is given by the following deviatoric stress–stretch relation:

$$\mathbf{T}_B = \frac{1}{J_B}C_R\frac{\sqrt{\bar N}}{\bar\lambda_N}\ell^{-1}\left(\frac{\bar\lambda_N}{\sqrt{\bar N}}\right)[\bar{\mathbf{B}}^N - (\bar\lambda_N)^2\mathbf{I}] \tag{11}$$

where J_B, N, and C_R are the network volume change, the number of rigid links between the entanglements, and the rubbery modulus, respectively. Also, ℓ^{-1} is the inverse Langevin function, given by $\ell^{-1}(x) = \coth(x) - (1/x)$. The stretch on each chain in the network, $\boldsymbol{\lambda}_N$, is given by $\boldsymbol{\lambda}_N = [1/3tr(\mathbf{B}^N]^{1/2}$ where $\mathbf{B}^N$ is equal to $\mathbf{F}_B(\mathbf{F}_B)^T$, $\mathbf{F}_B$ is equal to $(J_B)^{-1/3}\mathbf{F}_B$, and$\mathbf{F}_B$ is known from the Finite Deformation section.

Strain-induced crystallization

If we denote by ϕ_∞ the maximum degree of crystallinity, the crystallinity, ϕ, and the rate of crystallization are given by

$$\phi = \phi_\infty y, \quad \phi = \phi_\infty\dot y \tag{12}$$

where y is the degree of transformation. The rate of transformation is expressed with a phenomenological expression derived by Doufas et al.[7] on the basis of the Avrami equation and then modified by Ahzi et al.[13] to account for the strain rate. The evolution equation of the rate of transformation, $\dot y$, as a function of the developed Cauchy stress, $\mathbf{T}$, and the composite shear modulus, G_{com}, can be expressed as follows:

$$\dot y = \frac{dy}{dt} = \frac{\dot\varepsilon_{\mathrm{eq}}}{\dot\varepsilon_{\mathrm{ref}}}mK_{\mathrm{av}}(\theta)[-\ln(1-y)]^{(m-1)/m} \times (1-y)\exp\left(\zeta\frac{tr\mathbf{T}}{G_{\mathrm{com}}}\right) \tag{13}$$

where m is the Avrami exponent, ζ is a dimensionless model parameter, θ is the test temperature, $\dot\varepsilon_{\mathrm{eq}} = dv_z/dz$ is the applied equivalent strain rate, $\dot\varepsilon_{\mathrm{ref}}$ is a

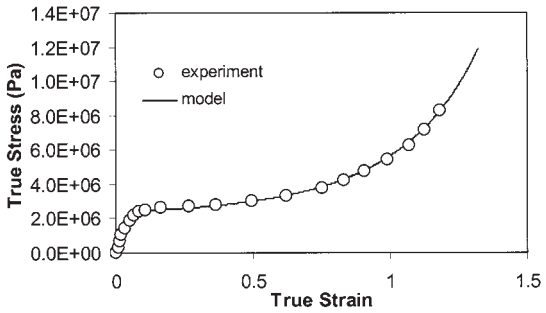

Figure 3 Stress–strain response at a strain rate of 0.08 s^{-1} in comparison with the experimental results at 25°C.

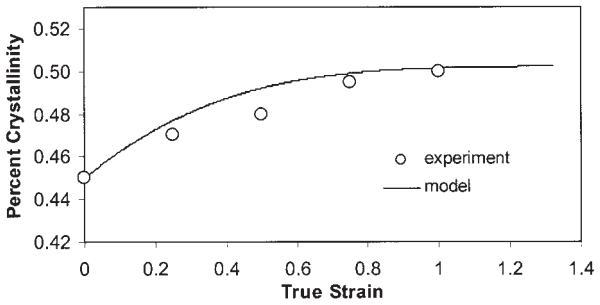

Figure 4 Crystallinity versus the true strain at a strain rate of 0.08 s^{-1} in comparison with the experimental results at 25°C.

reference strain rate, and $K_{av}(\theta)$ is the transformation rate function:

$$K_{av}(\theta) = K_{max}\exp\left(- 4\ln 2\frac{\theta - \theta_{max}}{D_{av}}\right) \quad (s^{-1}, \theta \text{ in } °C) \quad (14)$$

NUMERICAL METHOD

A one-dimensional finite-element discretization of the momentum and the energy equation is used to solve for the velocity and temperature, at each iteration, with Newton's method. The resulting temperature and velocity at each node are used to solve for the stress [eqs. (7)–(11)] and the degree of transformation [eq. (13)]. The two variables needed for the calculation of the total stress, $\mathbf{T} = \mathbf{T}_A + \mathbf{T}_B$, are the temperature and the strain rate, $\dot{\varepsilon}_{eq}$. The strain rate entering eq. (9) is the variation of the velocity in the axial direction. The stress and degree of transformation are calculated explicitly, element by element. Once the velocity gradient tensor [eq. (9)] is calculated, the deformation gradient, **F**, needed for the calculation of the stress, **T**, is determined explicitly: $\mathbf{F}_{t+\Delta t} = \mathbf{F}_t + \mathbf{LF}\Delta t$. Each element degree of transformation, $\dot{\phi}$, and total gradient of deformation, **F**, are used as the initial input for the next element. The strain rate, $\dot{\varepsilon}_{eq}$, and temperature, θ, at each element are taken as an average of the corresponding element's nodes.

In the first iteration, the stress components entering the momentum and the energy equations are taken to be zero.

RESULTS AND DISCUSSION

To verify the described model, we chose isotactic polypropylene (iPP) because the experimental data needed for the calibration of the constitutive equation (see the Governing Equations section) could be found in the Center for Advanced Engineering Fibers & Films (CAEFF) database.[16] To determine the model parameters for the iPP material, a uniaxial tension test was performed on a single iPP fiber at a temperature, θ = 35°C, above the glass-transition temperature and at a constant strain rate, $\dot{\varepsilon} = 0.08^{-1}$. The predicted true-stress/true-strain response (see Fig. 3) and the crystallinity percentage (see Fig. 4) were compared with our experimental data[16] to fit the model parameters. The true-stress/true-strain curve exhibits the four characteristic regions of a polymeric material above the glass-transition temperature. Under small deformation, the material exhibits a relatively stiff modulus, followed by a rollover to flow around 2.5 MPa. At a moderate deformation, the material shows gradual stiffening followed by a dramatic hardening at a large deformation.

The model parameters and physical properties of iPP are shown in Tables I and II. These parameters are used in the constitutive equation (see the Governing Equations section), which is coupled with the mass equation, momentum equation, energy equation, and boundary conditions to predict the fiber property profiles during the postdrawing. In Figures 5, 6, 9, and 10 (shown later), we present the results for the fiber length between the take-up (ℓ = 0 m) and ℓ = 2 m because these variables remain constant for the rest of the fiber length.

TABLE I
Fiber Stretch Parameters

Parameter	Value	Equation
V	4.6622×10^{-29}	(7)
n	3.65	(7)
$\dot{\gamma}_0$	2.25×10^7	(8)
ΔH_β	1.08×10^4	(8)
θ	25°C	(7), (8), and (13)
ν	0.43	(9)
C_R	0.15 MPa	(11)
N	9 MPa	(11)
$\dot{\varepsilon}_{eq}$	0.08 s^{-1}	(13)
$\dot{\varepsilon}_{ref}$	1.7 s^{-1}	(13)
ϕ_∞	0.7	(12)
K_{max}	0.55	(14)
θ_{max}	65°C	(14)
D_{av}	60°C	(14)

TABLE II
Postspinning Draw Parameters

iPP property	Value	Equation
ρ	0.85 g/cm^3	(1)
s	35 dyn/cm	(2)
C_{s1}	0.2502 cal/g °C	(4) and (6)
C_{s2}	7×10^{-4} cal/g °C^2	(4) and (6)
C_{s3}	0 cal/g °C^3	(4) and (6)
C_{l1}	0.3243 cal/g °C	(4) and (6)
C_{l2}	5.65×10^{-4} cal/g °C^2	(4) and (6)
C_{l3}	0 cal/g °C^3	(4) and (6)
v_y	0 m/s	(5)
ΔH_f (0)	30 cal/g	(6)
Processing parameters		
W	1.3345×10^{-6} kg/s	(1) and (2)
r_0	0.08 m	(2)
θ_a	25°C	(3)

The final fiber mechanical and structural properties are mainly related to the draw ratio (DR) between the draw roll and take-up roll velocities. The initial fiber velocity (take-up roll velocity) is 80 m/s. The relax roll is set to the same velocity as the draw roll to allow the fiber to relax. In Figure 5, the profile of the fiber strain rate versus its length is shown for DR = 2 and for different initial fiber equivalent stresses (the initial fiber stress is the fiber stress at the take roll developed between the spinneret and take-up roll). The strain rate increases dramatically close to the take-up roll and then decreases nonlinearly to zero on the draw roll. The strain-rate peak close to the take-up roll is due to the unbalanced forces between the inertial force and the tensile force. A higher tensile stress causes the inertial force in the fiber, which originates at the draw roll, to dissipate more quickly. Indeed, a higher fiber initial stress results in higher overall fiber stress, which results in a lower strain-rate peak. The peak height is also a function of the DR between the draw roll and the take-up roll. For the same equivalent initial stress, T_{init} = 0.5 MPa, the peak height drops

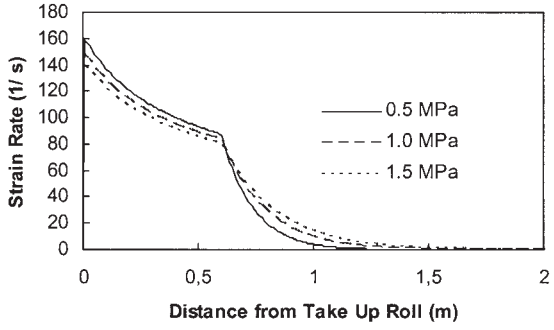

Figure 5 Predicted profile of the fiber strain rate (s^{-1}) for different fiber initial equivalent stresses (stresses at the take-up roll) and at a roll temperature of 35°C.

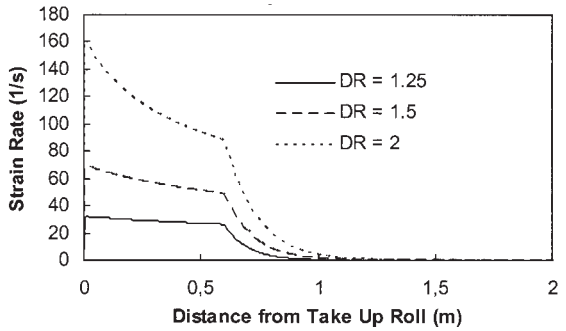

Figure 6 Predicted profile of the fiber strain rate (s^{-1}) for different DRs between the draw roll and take-up roll at a roll temperature of 35°C.

significantly when the DR decreases (see Fig. 6). In fact, the lower the fiber DR is, the lower the fiber strain is, and this leads to lower inertial force and a lower peak. Control of the strain rate close to the take-up roll can be used to avoid fiber breakage, which may result from significant acceleration in this region. After the peak, the strain-rate curve shows two different regions with two different slopes before vanishing to zero. The first region represents the fiber strain rate between the take-up roll and the draw roll, and the second region represents the fiber on the draw roll. The second region shows the fiber sliding length before its velocity reaches the draw roll velocity. This length depends on the take-up velocity and the fiber stress level. The strain rate [Figs. 6(a) and 7] vanishes when the fiber velocity reaches the draw roll velocity.

Figure 7 illustrates the contribution of the network resistance and intermolecular resistance to the total fiber stress in the postdrawing process for DR = 2 and T_{init} = 0.5 MPa. The fiber stretching between the take-up roll and the draw roll increases the intermolecular and network resistances, and this results in the increase in the overall fiber stress. On the draw roll, the fiber stress decreases and then becomes constant when the strain rate is zero. The network resistance in Figure

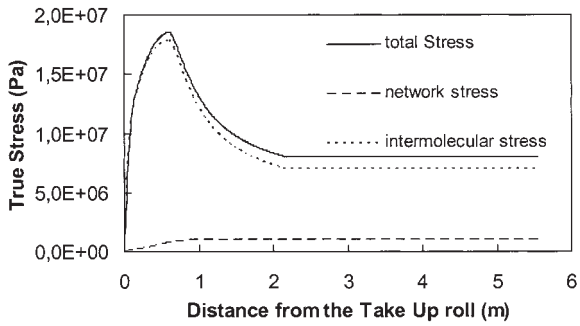

Figure 7 Contribution of the network resistance and the intermolecular resistance to the fiber total true stress for DR = 2 at a roll temperature of 35°C and an initial fiber equivalent stress of 0.5 MPa.

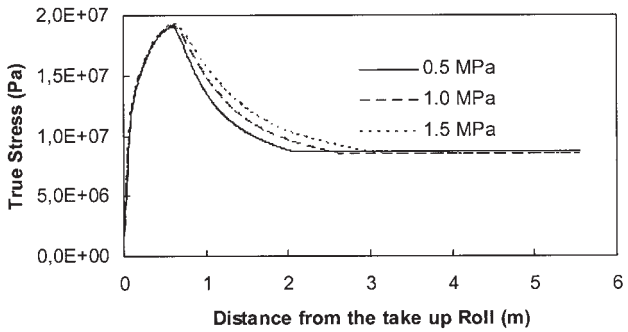

Figure 8 Fiber stress–strain profile for different fiber initial equivalent stresses at a roll temperature of 35°C and at DR = 2.

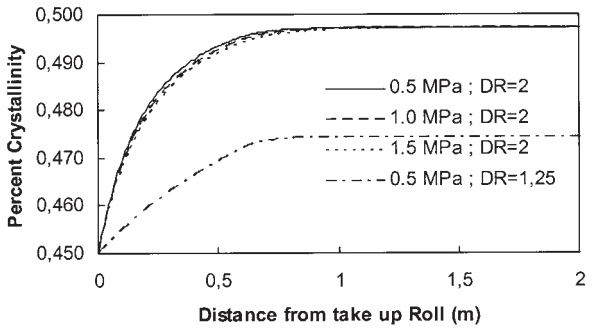

Figure 10 Fiber crystallinity for different fiber equivalent stresses and DRs at a roll temperature of 35°C.

7 shows a small variation in the region in which strain rate drops rapidly because of the slow variation of the fiber total deformation gradient, which in turn allows the molecular chains of the amorphous phase to relax and decreases the intermolecular resistance.

The effect of the fiber initial stress on the fiber total stress under a DR of 2 is shown in Figure 8. With an increase in the initial stress, the curves of the total stress move higher, and this leads to stiffer fibers. Consequently, higher fiber stiffness results in weaker friction on the draw roll, which increases the sliding distance. The constant total stress after the intermolecular relaxation marks the end of the sliding distance. This behavior is reflected in the fiber velocity curves (see Fig. 9): the fiber with high stress shows a low velocity and a longer sliding distance. The limit of the sliding distance on the draw roll is achieved when the strain rate vanishes at the moment at which the fiber velocity becomes equal to the draw roll velocity.

The effects of the DR and the fiber stress level on the crystallinity percentage for T_{init} = 0.5 MPa are shown in Figure 10. A higher DR results in a higher fiber crystallinity percentage because of the high amount of deformation. For the same DR of 2, the curves in Figure 10 show that the rate of crystallization decreases when the initial stress increases and the strain rate decreases (see Fig. 5), and this agrees with the experimental results of Salem.[17,18] The curves converge to the same value after the fiber velocity reaches the imposed DR, suggesting that the final fiber crystallinity percentage depends on the amount of deformation but not on the history of the deformation.

The fiber temperature profile is shown in Figure 11 for two different DRs with the same T_{init} value (0.5 MPa). The temperatures of the take-up roll, draw roll, and relax roll are set to 35°C. Between the take-up roll and draw roll, the decrease in the fiber temperature due to convective heat transfer is limited by the gain of heat from the fiber's plastic deformation. Between the draw roll and the relax roll, the fiber plastic deformation is zero, and the only fiber heat transfer is by convection. With an increase in the DR, the temperature change between the take-up roll and draw roll is due to the change in the convection coefficient, which is a function of the fiber velocity and fiber diameter. Between the take-up roll and draw roll, in addition to the change in the convection coefficient, there is an increase in the heat gain with the fiber plastic deformation. As can be seen in eq. (3), the total plastic work is assumed to be converted to heat.

CONCLUSIONS

We have successfully implemented a model for the simulation of fiber postdrawing, coupling a polymeric constitutive equation for finite deformation with the mass

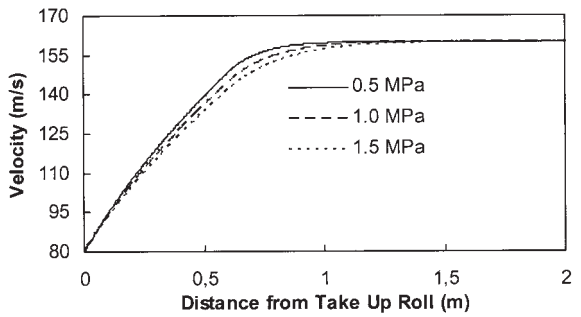

Figure 9 Fiber velocity profile for different fiber equivalent initial stresses at a roll temperature of 35°C and at DR = 2.

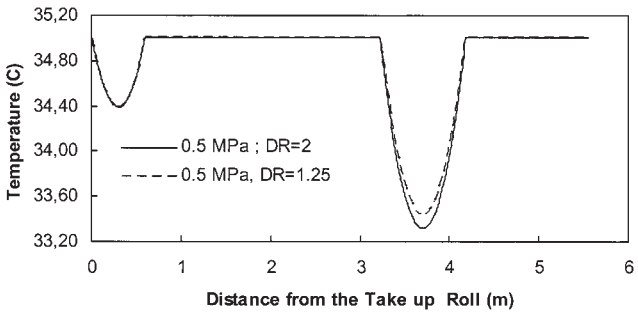

Figure 11 Fiber temperature profile for different DRs at a fiber initial equivalent stress of 0.5 MPa and a roll temperature of 35°C.

balance, momentum balance, energy and rate of crystallization equations. The simulations were conducted with a one-dimensional finite-element method. However, the constitutive relations are three-dimensional. The predicted results show a strong dependence of the fiber strain rate close to the take-up roll on the DR and fiber stress level in this region. Close to the take-up roll, a fiber with high stiffness and a low DR develops a low strain-rate peak, which helps to prevent fiber breakage. On the draw roll, the sliding distance depends on the fiber stress level. Higher fiber stiffness results in a higher sliding distance. The final fiber crystallinity percentage depends on the amount of deformation and not on the history of the deformation. The fiber temperature is governed by the heat loss by convection and heat gain by fiber plastic deformation. Between the take-up roll and draw roll, plastic deformation plays the important role of limiting the fiber temperature decrease by convective heat transfer. Between the draw roll and the relax roll, the fiber does not deform, and the only heat transfer is by convection, which depends on the DR as the convection coefficient depends on the fiber velocity and diameter.

The authors thank Amit Naskar of Clemson University for the experimental data on the crystallization percentage.

References

1. Argon, A. S. Philos Mag 1973, 28, 839.
2. Richeton, J.; Ahzi, S.; Daridon, L.; Rémond, Y. J Phys IV 2003, 110, 39.
3. Richeton, J.; Ahzi, S.; Daridon, L.; Rémond, Y. Polymer 2005, 46, 6035.
4. Bechtel, S. E.; Vohra, S.; Jacob, K. I. Polym Eng Sci 2004, 44, 312.
5. Bechtel, S. E.; Vohra, S.; Jacob, K. I. Polymer 2001, 42, 2045.
6. Denn, M. M. In Computational Analysis of Polymer Processing; Pearson, J. R. A.; Richardson, S. M., Eds.; Applied Science: London, 1983; p 179.
7. Doufas, A. K.; McHugh, A. J.; Miller, C. J Non-Newtonian Fluid Mech 2000, 92, 27.
8. Ziabicki, A.; Jarecki, L.; Wasiak, A. Comput Theor Polym Sci 1998, 8, 143.
9. Fotheringham, D.; Cherry, B. W. J Mater Sci 1976, 11, 1368.
10. Bauwens-Crowet, C.; Bauwens, J. C.; Homès, G. J Polym Sci A-2: Polym Phys 1969, 7, 735.
11. Ree, T.; Eyring, H. J Appl Phys 1955, 26, 793.
12. Boyce, M. C.; Socrate, S.; Llana, P. G. Polymer 2000, 41, 2183.
13. Ahzi, S.; Makradi, A.; Gregory, R. V.; Edie, D. D. Mech Mater 2003, 33, 1139.
14. Arruda, E. M.; Boyce, M. C. J Mech Phys Solids 1993, 41, 398.
15. Arruda, E. M.; Boyce, M. C. Int J Plast 1993, 9, 607.
16. http://caeff.ces.clemson.edu/physical/index.php.
17. Salem, D. R. Polymer 1992, 33, 3182.
18. Salem, D. R. Polymer 1994, 35, 771.